Fuel-efficient Descent and Landing Guidance Logic for a Safe Lunar Touchdown

Allan Y. Lee*
Jet Propulsion Laboratory, California Institute of Technology, Pasadena, California

Abstract

The landing of a crewed lunar lander on the surface of the Moon will be the climax of any Moon mission. At touchdown, the landing mechanism must absorb the load imparted on the lander due to the vertical component of the lander's touchdown velocity. Also, a large horizontal velocity must be avoided because it could cause the lander to tip over, risking the life of the crew. To be conservative, the worst-case lander's touchdown velocity is always assumed in designing the landing mechanism, making it very heavy. Fuel-optimal guidance algorithms for soft planetary landing have been studied extensively. In most of these studies, the lander is constrained to touchdown with zero velocity. With bounds imposed on the magnitude of the engine thrust, the optimal control solutions typically have a "bang-bang" thrust profile: the thrust magnitude "bangs" instantaneously between its maximum and minimum magnitudes. But the descent engine might not be able to throttle between its extremes instantaneously. There is also a concern about the acceptability of "bang-bang" control to the crew. In our study, the optimal control of a lander is formulated with a cost function that penalizes both the touchdown velocity and the fuel cost of the descent engine. In this formulation, there is not a requirement to achieve a zero touchdown velocity. Only a touchdown velocity that is consistent with the capability of the landing gear design is required. Also, since the nominal throttle level for the terminal descent sub-phase is well below the peak engine thrust, no bound on the engine thrust is used in our formulated problem. Instead of bang-bang type solution, the optimal thrust generated is a continuous function of time. With this formulation, we can easily derive analytical expressions for the optimal thrust vector, touchdown velocity components, and other system variables. These expressions provide insights into the "physics" of the optimal landing and terminal descent maneuver. These insights could help engineers to achieve a better "balance" between the conflicting needs of achieving a safe touchdown velocity, a low-weight landing mechanism, low engine fuel cost, and other design goals. In comparing the computed optimal control results with the preflight landing trajectory design of the Apollo-11 mission, we noted interesting similarities between the two missions.

Nomenclature

ALHAT	Autonomous Landing Hazard Avoidance Technology
Altair	Lunar Lander Vehicle
AM	Ascent Module

* Section staff in the Jet Propulsion Laboratory Guidance and Control Section, 4800 Oak Grove Dr., M.S. 230-104, Pasadena, CA 91109-8099. AIAA member. Manager, Guidance, Navigation, and Control Subsystem, Altair Lunar Lander Project, 2007–2010.

ARES-I	Launch vehicle for Orion
ARES-V	Launch vehicle for Altair
B/U	Backup
DM	Descent Module
EVA	Extravehicular Activity
FOV	Field of view (of an optical sensor or radar)
GET	Ground Elapsed Time (from Liftoff)
GN&C	Guidance, Navigation, and Control subsystem
IMU	Inertial Measurement Unit
JPL	Jet Propulsion Laboratory
JSC	Johnson Space Center
Lidar	Light Intensification, Detection, and Ranging
LIDS	Low Impact Docking System
LLO	Low Lunar Orbit
LOC	Loss of Crew
LOM	Loss of Mission
NAC	Narrow Angle Camera
NASA	National Aeronautics and Space Administration
ONSS	Optical Navigation Sensor System
OpNav	Optical Navigation
Orion	Crew Exploration Vehicle
PDI	Powered Descent Initiation
RCS	Reaction Control System
S/C	Spacecraft
SRU	Stellar Reference Unit (usually called a Star Tracker)
TBD	To Be Determined
TD	Touchdown
TDRS	Terminal Descent Radar System
THDSS	Terrain Hazard Detection Sensor System
TPBVP	Two Point Boundary Value Problem
TVC	Thrust Vector Control (a ΔV burn performed by a gimbal engine)

I. The Altair Lunar Lander Mission

THE Constellation Program[+] is NASA's response to the human exploration goals set by former President George W. Bush for returning humans to the Moon by 2020. In January 2004, former President Bush announced the new Vision for Space Exploration for NASA. The fundamental goal of this vision is to advance U.S. scientific, security, and economic interests through a robust space exploration program. To this end, the NASA Constellation Program is working on two spacecraft (the Crew Exploration Vehicle named Orion and the Lunar Lander Vehicle named Altair), two launch vehicles (ARES-I will launch Orion and ARES-V will launch Altair), and surface support systems to establish a lunar outpost. This work will provide experience needed to expand human exploration farther into the Solar System.

The Lunar Lander Altair is the linchpin in the Constellation Program for human return to the Moon. In the spring of 2007, a small group of engineers from multiple NASA centers were assembled in Houston, Texas to kick off the first design cycle of the lunar lander.[†] In this cycle, the team focused on the establishment of a "minimal functionality" vehicle design for a polar sortie mission. After six months of work, with many collocations of team members at JSC, the team created a viable but "single string" design. This "minimal functionality" design provides no redundancy and has no provision for most contingencies. One failure and you lose the mission. NASA did not intend to fly anything like this stripped-down Altair, but the concept enabled the team to produce a design that copes with the immutable physics of executing a lunar landing. Decision makers can then consciously add safety and reliability features with full knowledge of how much risk reduction those enhancements are buying.

[†] The future of the human space flight program, and thus the Constellation program, is currently being discussed at the highest levels of the U.S. government. This paper is written without consideration of any forthcoming changes in the direction (or even existence) of the program.

After the "minimal functionality" design cycle was concluded, two additional design cycles (cycles 2 and 3) were performed in 2008 to improve the resiliency of the minimal-functionality design relative to, first the "Loss of Crew" (LOC) and then the "Loss of Mission" (LOM) risks. This was achieved via selective addition of vehicle functionality, new sensors, and redundancy of selected equipment. In addition to the sortie lander, the Altair team also studied two other lander variants: an outpost lander and a cargo lander. The outpost Altair would execute seven-month missions to a future lunar base. The unpiloted cargo Altair would have neither an ascent module nor an airlock. Other works done by the lander design team in 2009–10 were described in Lee et al. (2010).[1]

The lunar lander vehicle Altair design is a three-axis stabilized spacecraft. Three-axis stabilized spacecraft are best suited to missions where a high degree of maneuverability is required. Like the Apollo Lunar Lander designs, Altair consists of a descent module and an ascent module. The descent module (DM) is the unmanned portion of Altair. It carries the large descent main propulsion engine, and eight propellant tanks. It also carries a set of RCS thrusters. The DM also provides structural supports for both the ascent module and the landing gear. The landing gear provides the impact attenuation required to land Altair on the lunar surface, preventing vehicle tip-over at touchdown. The entire descent module is enveloped in a thermal and micro-meteoroid shield. The ascent module (AM) has a crew compartment that provides a controlled environment for up to four astronauts. The sortie lander, depicted in Fig. 1, carries an airlock for surface extravehicular activity (EVA). Crews reside in the ascent module at times of lunar landing and docking with Orion. Crew visibility of the landing site is via the two forward windows. Visibility to Orion at time of docking is via the two top windows. Near the top of the module is the passive side of the Low Impact Docking System (LIDS) adapter. Three Altair/Orion S-band radio antennas are also mounted near the top of the ascent module. The ascent module carries the ascent main propulsion engine and the associated fuel tanks. It also carries a set of RCS thrusters.

The Guidance, Navigation, and Control (GN&C) system must perform many functions that are critical to the Altair mission. To perform these GN&C functions, a set of GN&C sensors is selected. The functions performed by these sensors are described briefly in the following paragraphs. Details are given in Ref. 1. The placements of these sensors are depicted in Fig. 1.

The spacecraft's attitude in a celestial frame is estimated using a Stellar Reference Unit (SRU, sometimes called a star tracker) and a set of three gyroscopes. The primary star tracker is mounted on the AM. The backup star tracker and a narrow angle camera are mounted on a 2-dof gimbal platform. This sensor package, named Optical Navigation Sensor System (ONSS), is specifically included in the GN&C sensor suite for the purpose of performing optical navigation.[2] All Constellation elements are required to "get the crew home" even when communications links are down or degraded. This ensures the safety of the crew by allowing the Constellation systems to still function adequately if there were permanent or unplanned intermittent communication service outages preventing or limiting the ability of mission systems to interface with the vehicles used for the given mission.

Three Inertial Measurement Units (IMU) are included in the Altair GN&C sensor suite. The primary IMU contains four gyroscopes and four accelerometers. The two backup IMUs are identical, and each unit contains three gyroscopes and three accelerometers. Measurements from three selected prime gyroscopes are used to support the attitude determination function. Measurements from three selected prime accelerometers are used to support the propagations of spacecraft's "state" vector (the position and velocity vectors of the spacecraft).

For guidance and control of Altair in the descent and landing phase, a Terminal Descent Radar System (TDRS) is used to estimate the surface-relative Altair's altitude and velocity. In the general vicinity of the intended landing site of Altair, near the lunar South Pole, there are many terrain hazards that will be challenging to the Altair's landing gear. These hazards include craters, slopes, and rocks. For Altair, a sensor named Terrain Hazard Detection System Sensor (THDSS) is the primary mean of terrain hazard detection.[3] Crew visual detection is the backup (via out-the-window viewing). The THDSS is modeled after a sensor that is being developed under a technology program named Autonomous Landing Hazard Avoidance Technology (ALHAT).[4,5] As a placeholder, THDSS will consist of a flash Light Intensification, Detection, and Ranging (lidar) that is mounted on a 2-dof gimbaled platform.

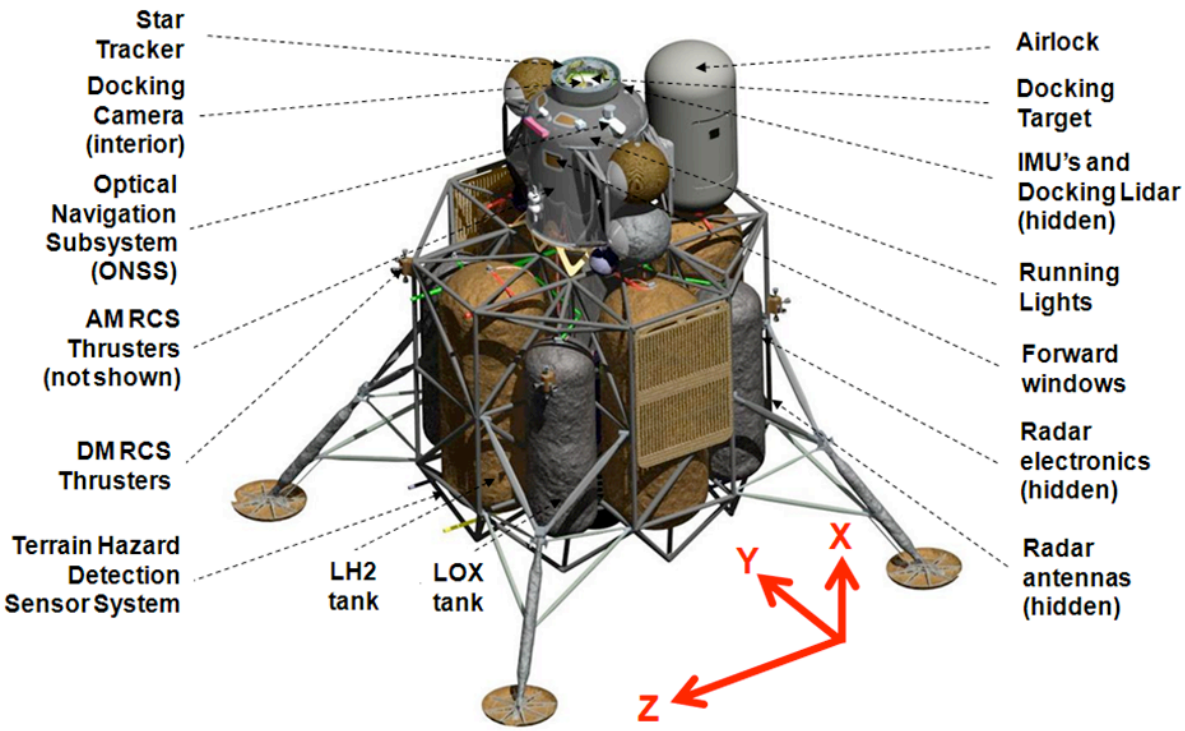

Fig. 1. The Altair lunar lander vehicle ("Sortie" lander).[1]

The rendezvous and docking process consists of a series of orbital maneuvers and spacecraft attitude control motions that successively bring the active vehicle into the vicinity of, and eventually into contact with, the passive vehicle.[6] Fundamental to the set of rendezvous and docking sensors are the star tracker and the IMU. In the current GN&C plan, the bearing angles from the Altair AM to Orion are estimated using the prime star tracker. As a backup, the cameras of ONSS are used. The range and range-rate between the two vehicles is estimated via the two-way S-band radiometric ranging data. Again, as a backup, they could also be estimated using the ONSS cameras. Once the vehicles are within a range of 4–5 km, estimates of the bearing angles and range with better accuracy could be provided by a scanning lidar (Laser Imaging, Detection, and Ranging). Once the vehicles are within 100–150 m, lidar also provides estimates of the relative attitude of Altair and Orion (also called "pose").

Lunar descent guidance begins with Altair at an altitude of 15.24 km in a slightly elliptical coasting lunar orbit, and it ends with Altair on the lunar surface. The objective of the guidance is to reduce both the velocity and altitude of Altair for a soft touchdown at the selected landing site. Guidance in this phase is designed based on the following considerations:

- Minimize propellant usage
- Maximize landing accuracy
- Provide "out-the-window" line-of-sight to the landing site for the crew several minutes before touchdown
- Provide line-of-sight to the general landing area for the gimbaled THDSS carried onboard Altair
- Allow for re-designation of the landing site several minutes before touch down

These considerations are almost identical to those faced by the GN&C engineers of Apollo missions. Hence, not surprisingly, the descent guidance trajectory of Altair is very similar to those used by the Apollo missions.[7–10] The Altair descent guidance design consists of three sub-phases: the braking phase, the approach phase, and the terminal descent and touchdown phase. These descent sub-phases are depicted in Fig. 2.

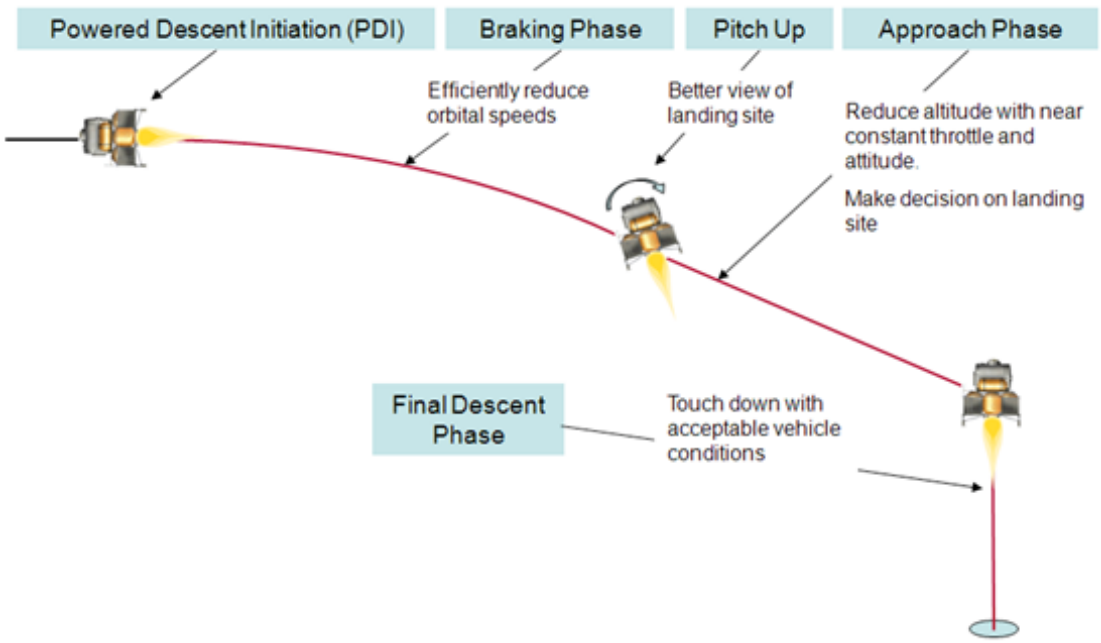

Fig. 2. Sub-phases in the Descent and Landing Phase.[11]

The basic guidance law assumes a 4th-order polynomial function (of time) that describes the desired trajectory in position. The guidance equations are solved by posing Two-Point Boundary-Value-Problems (TPBVP).[5,7] Different target sets are used for different sub-phases of the descent and landing phase. The braking sub-phase is initiated by the crew about 10 min. before the nominal ignition of the descent engine. It starts at the descent orbit perilune at an altitude of 15.24 km. The objective of the braking burn is to efficiently reduce the orbital speed of Altair.

In the Approach sub-phase, the throttle is lowered to a level that is about 60% of the full engine thrust. The very first control action is to perform a pitch-up maneuver, changing the vehicle's attitude from nearly horizontal to nearly vertical. This allows the crew to gain a better view of the targeted landing site. This is important because re-designation of the landing target, if any, must be performed in the approach phase. The crew is assisted by the THDSS system to make a decision on whether there is a need to re-designate and on the selection of the safe landing site(s). Undesirable horizontal velocity of the vehicle in this phase could be nulled out using the RCS thrusters. Alternatively, RCS thrusters could be used to pitch (or roll) the vehicle's attitude (slightly forward or backward, or left/right) so that some component of the engine thrust could null the horizontal forward and/or lateral velocities.

The terminal sub-phase is intended to be a quiescent, controlled, vertical descent for 30 s from an altitude of about 30 m, at a constant 1 m/s vertical descent rate, until it is time to shut down the DM engine. Engine shut down occurs just prior to touch down. For Apollo missions, engine shutdown was performed manually when 1.7-m contact probes touched the ground and a light was activated in the cockpit. The Altair landing gear does not currently include similar probes. The tentative plan is to estimate altitude via IMU-propagation of the last good radar measurement.

A. Focusing on the Landing Phase

The basic purpose of the landing phase is provide a period of flight at low velocities and at pitch attitudes close to the vertical so that the pilot can provide vernier control of the touchdown (TD) maneuvers and also to have the opportunity for a final assessment of the landing area prior to the TD. Constraints faced by the Crews in the landing phase include efficient fuel utilization, window and lighting visibility, the presence of dust clouds, and the presence of terrain hazards at touchdown.

Nominally, near the starting point of the landing and terminal descent sub-phase, the lander must satisfy a set of so-called "low gate" conditions. For Apollo missions, representative low-gate conditions have an altitude of 155 m, a downrange distance of 370 m from the intended TD site, a horizontal velocity of 16–17 m/s, a vertical velocity of 4.6–4.8 m/s (downward), and a pitch angle is 10–16°.[7,12] The flight path is shaped to reach a "state" (called Terminal Descent Initiation (TDI) state) with an altitude of about 30 m above the landing spot with nearly zero forward

velocity from which a purely vertical descent can be initiated. At the TDI state, the vertical velocity might still be about 1–1.5 m/s (downward). The nominal maneuver time, from the low-gate to touch down, is 80 s. The actual "low-gate" conditions of several Apollo missions are listed in Table 1.[8–10]

Table 1. Apollo Vehicles at Low-gate and TD States[8–10]

Missions	Low-Gate Velocity [Horizontal, Vertical] m/s	Low-Gate Rates [X, Y, Z] deg/s [pitch, roll, yaw]	Low-Gate Altitude m	TD Velocity [Horizontal, Vertical] m/s	TD Rates [X, Y, Z] deg/s [yaw, pitch, roll]	TD Attitude [roll, pitch] deg
Apollo-11	18.3, -3.1	2, 2, Unknown	125	0.6, 0.3	0.6, 0.6, 1.6	2.6, 0.8
Apollo-12	24, -2.7	-6.3, 7.6, -4.6	123	0.6, 0.9	4.3, 19.5, 7.8	0.35, 1.4
Apollo-14	10.5, -3.4	-4.3, -7.1, 4.1	86	0.6, 0.6	1.4, 2.7, 1.3	Unknown
Apollo-15	9.1, -3.6	Unknown	101	0.3, 2	14.2, 0.52, 2.5	Unknown

Perhaps the most important single operation in the lunar landing mission is the actual TD maneuver. The landing gear of the lander must provide sufficient energy absorption capability and adequate vehicle-toppling stability for a range of lunar surface characteristics, and for a range of vehicle TD conditions. For the Apollo-11 lander, the maximum allowable horizontal and vertical TD velocities are given by (V_H and V_V are the magnitudes of the horizontal and vertical TD velocities, in m/s, with respect to the Moon gravity vector):[13–14]

$$\begin{aligned} &\text{For } 0 \le V_V \le 2.13, && \text{peak } V_H \le 1.22; \\ &\text{For } 2.13 < V_V \le 3.05, && \text{peak } V_H \le 4.045 - 1.326 \times V_V; \\ &\text{For } 3.05 < V_V, && \text{Not acceptable} \end{aligned} \tag{1}$$

The corresponding 3σ limits of the pitch and roll angles (from the local vertical) are 6° per axis. The 3σ limits of the pitch and roll rates are 6 °/s per axis (as per Ref. 13. But the rate limit as documented in Ref. 14 is 1.5 °/s). Actual TD conditions for several Apollo missions are listed in Table 1. Acceptable TD conditions for the Altair's landing gear design are work-in-progress.

The baseline ΔV budget (descent engine) for the landing phase of Apollo missions is 119 m/s. Contingency ΔV allowances (e.g., inspection of the landing site via hovering) summed to about 100 m/s. In Ref. 11, the ΔV budgeted for the combined Approach and Landing phases of the Altair lander was 217 m/s (descent engine). This is reasonably consistent with the Apollo allocation of 119 m/s (for the Landing phase). The contingency ΔV budget (for the descent engine) of Altair is 58 m/s (re-designation of the landing site and dispersion of system variables).[11] The ΔV budget for the RCS thrusters for the entire powered descent and landing phase estimated to be 11 m/s.[11]

II. Optimal Terminal Descent Guidance Logic

The landing of a crewed lunar lander on the surface of the Moon will be the climax of any Moon mission. At touchdown, the landing mechanism must absorb the load imparted on the lander due to the vertical component of the lander's touchdown velocity. Also, a large horizontal velocity could cause the lander to tip over, risking the life of the crew. To be conservative, worst-case lander's touchdown velocity is always assumed in designing the landing mechanism, making it very heavy. To achieve a good "balance" between the conflicting needs of achieving a safe touchdown velocity, a low-weight landing mechanism, low engine fuel cost, and other requirements is not easy. Simple expressions that related the key figures of merit (e.g., the TD velocity and fuel cost) with key flight variables including the vehicle's state at the start of the landing phase, the descent time, and others could be very useful to the systems engineers of the vehicle integration team. The derivation of these expressions is one goal of this study.

Fuel-optimal guidance algorithms for soft planetary landing had been studied extensively. In most of these studies, the lander is constrained to TD with zero velocity. With bounds imposed on the magnitude of the engine

thrust, the optimal control solutions typically have a "bang-bang" thrust profile: the thrust magnitude "bangs" instantaneously between its maximum and minimum magnitudes. But the descent engine might not be able to execute these optimal programs effectively. There is also a concern about the acceptability of "bang-bang" control to the crew. In our study, the optimal control of a lander is formulated with a cost function that penalizes both the TD velocity and the fuel cost of the descent engine. In our formulation, there is no requirement to achieve a zero TD velocity. Only a TD velocity that is consistent with the capability of the landing gear design is required. Also, since the nominal throttle level for the terminal descent sub-phase is well below the peak engine thrust, no bound on the engine thrust is used in our formulated problem. As a result, instead of bang-bang type solution, the optimal thrust program generated is a continuous function of time. Also, without a hard bound on the control thrust, we can easily derive analytical expressions for the optimal thrust vector, TD velocity components, and other system variables. These expressions provide insights into the "physics" of the optimal landing and terminal descent maneuver. These insights might help the systems engineers in achieving a good "balance" between the conflicting needs of achieving a safe TD velocity, a low-weight landing mechanism, low engine fuel cost, and other requirements.

In References 15 and 16, the landing of a helicopter in autorotation was formulated as a nonlinear optimal control problem with inequality constraints. The helicopter was modeled as a point-mass. The performance index is a weighted sum of the squares of vertical and horizontal velocities at touchdown. The control inequality constraint was a limit on the helicopter rotor thrust coefficient. The state inequality constraint was a limit on the vertical sink rate of the helicopter. The general approach taken in these references is followed in this study.

The descent and landing of the lander during descent is depicted in Fig. 3. The two-dimensional planner motion of the lander (which is modeled as a point mass) is governed by the following equations of motion.

$$\begin{aligned} \dot{x}_1 &= u_1 \\ \dot{x}_2 &= u_2 - g \\ \dot{x}_3 &= x_2 \\ \dot{x}_4 &= x_1 \end{aligned} \tag{2}$$

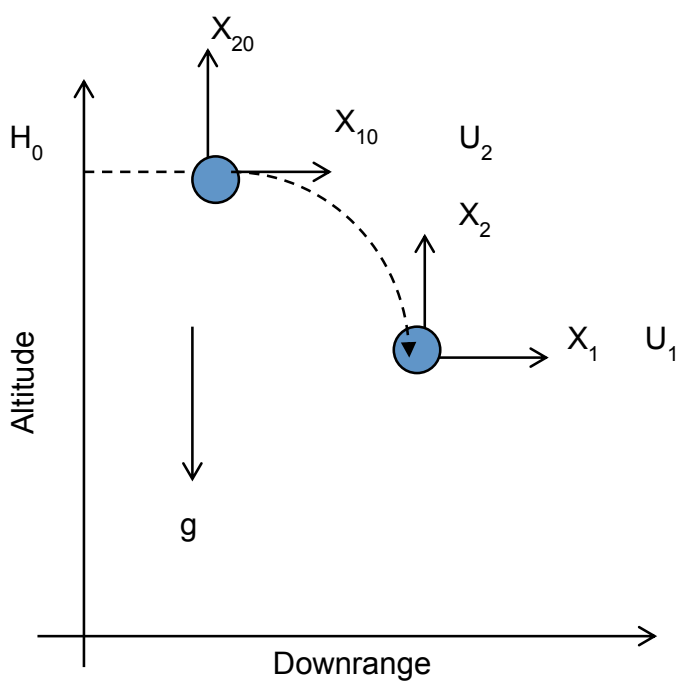

Fig. 3. Optimal control of a lander to ahieve a "soft" touchdown.

Here, x_1 is the lander's horizontal velocity (in m/s), x_2 is the lander's vertical velocity (in m/s), x_3 is the lander's altitude (in m), and x_4 is the lander's downrange (in m). The positive directions of these variables are depicted in

Fig. 3. The horizontal and vertical components of the gimbaled engine thrust are represented by F_1 (=mu_1) and F_2 (=mu_2), respectively. The engine thrust components normalized by the mass of the vehicle are denoted by u_1 and u_2 (in units of m/s^2). The positive directions of these thrust components are also depicted in Fig. 3. In this study, for simplicity, we assume that the mass of the lander is constant. This is obviously not true since fuel must be expended to generate thrust.[17–18] However, for the Altair lunar lander, the ratio of fuel consumed (from low-gate to touch-down) to the lander mass at touchdown is <5%,[1,11] which is small. Finally, g (in m/s^2) denotes the constant acceleration due to gravity of the Moon.

The initial conditions of x_1, x_2, and x_3 are denoted by x_{10}, x_{20}, and H_0, respectively. The final condition of x_3, at a pre-selected terminal TD time T (in units of s) is $x_3(T) = 0$ ("touch down"). The initial condition of x_4 is selected to be zero. In the first optimization problem formulated, the terminal condition of x_4 is unconstrained. In the next two formulated problems, there will be either a "hard" or "soft" constraint on the terminal state of x_4.

Consider the following optimization problem. The thrust components $u_1(t)$ and $u_2(t)$ ($T \geq t \geq 0$) are to be selected to minimize the following cost function J.

$$J = \frac{1}{2}[x_1^2(T) + x_2^2(T)] + \frac{W}{2}\int_0^T [u_1^2(t) + u_2^2(t)]\, dt \tag{3}$$

Physically, the first component of J is related to the lander's touchdown (TD) velocity. The unit of this term is m^2/s^2. The vertical velocity of the lander at touchdown is the primary factor used in sizing the energy absorbing devices of the lander. Hence, it has to be minimized. The horizontal velocity of the lander must also be minimized. When the lander touchdown "on the edge", the kinetic energy due to the forward velocity is converted into a rotational energy which might tip over the lander. The second component of J is related to the fuel the descent engine consumed in achieving a "safe" TD condition. Cost functions with similar squared control terms were also used in Refs. 19 and 21. For example, in Ref. 21, a closed-loop guidance law that minimizes the commanded squared-acceleration with a weighted final time was developed. The weighting parameter W in Eq. (3), in units of seconds, is used to sum together the two terms in the cost function. The weighting factor W should not be zero or else the optimal control problem is not well posed. The impacts of the weighting factor W on the lander's optimal TD velocity and the optimal fuel cost are depicted in Figures 5 and 6, respectively.

An alternative cost function that could have been used is

$$1/2\sqrt{x_1^2(T)+x_2^2(T)} + W/2\int_0^T \sqrt{u_1^2(t)+u_2^2(t)}dt$$

Again, the first term represents the magnitude of the lander's velocity vector at touchdown and the term under the integral represents the magnitude of the engine thrust. Obviously, it is harder to derive an analytical expression for the optimal control solution for this revised optimization problem (and the optimal solution must be computed numerically). Hence, the cost function given in Eq. (3) is used in our study.

Unlike the optimal control problems formulated in Refs. 17–22, we do not impose an upper bound on the magnitude of the engine thrust $\sqrt{u_1^2+u_2^2}$. The nominal value of the peak thrust of the Altair descent engine is 82,857 N.[1] The nominal throttle levels of the descent engine during the Braking, Approach, and Terminal Descent sub-phases are 92, 46, and 39%, resepectively.[3] We note that during the terminal descent phase, the nominal thrust level is well below the capability of the engine. Fuel-optimal control problems formulated with a bounded thrust typically generate thrust profile consists of "bang-bang" type control.[17–22] In these optimal thrust solutions, the thrust magnitude "bangs" instantaneously between its maximum and minimum magnitudes. Even ignoring for the time being whether the lunar lander descent engine can be throttled between its minimum and maximum thrust magnitudes instantaneously, we also have a concern about the acceptability of these types of bang-bang control for crew safety. To generate a simple and continuous thrust profile, we use the cost function given in Eq. (3) to limit the usage of fuel and the optimization problem is formulated without any hard bound on the thrust magnitude.

The formulated optimal control problem could be solved via the classical calculus of variations technique. See, for example, Chapter 3 of Reference 23. The solution approach is summarized as follows. Consider the following optimal control problem[23]

$$\begin{aligned} &\min_u J = \phi(x_f) + \int_0^{t_f} L(x(t),u(t),t)\ dt \\ &\dot{x}(t) = f(x(t),u(t),t),\ \ x(0) = \text{given}, \\ &\psi(x_f) = 0. \end{aligned} \tag{4}$$

Here x(n × 1) and u(m × 1) are the state and control vectors, ψ(q × 1) are terminal constraints, t is the independent variable, and $(\bullet)_f$ denotes the condition of the variable concerned at the end time t_f. The necessary conditions of the optimization problem are stated using the scalar functions H (the Hamiltonian function) and Ψ:

$$\begin{aligned}
&\dot{\lambda}^T = -H_x \\
&H_u = 0 \\
&\lambda_f^T = (\Psi_x)_f \\
&H(x,u,\lambda,t) = L(x,u,t) + \lambda^T f(x,u,t) \\
&\Psi(x_f,\mu) = \phi(x_f) + \mu^T \psi(x_f)
\end{aligned} \tag{5}$$

Here, λ is the Lagrange multiplier variable associated with f, μ is the Lagrange multiplier associated with ψ, and H_α and Ψ_β denote $\partial H/\partial\alpha$ and $\partial\Psi/\partial\beta$, respectively. Using the necessary condition given in Eq. (5), we can solve the dynamical optimization problem. For the optimization problem formulated in Eqs. (2) and (3), the resultant optimal control is given by:

$$\begin{aligned}
&u_1(t) = -K_1 = \text{constant} \\
&u_2(t) = K_2 t - K_3 = \text{ linear variation of time}
\end{aligned} \tag{6}$$

Here, the constants K_1, K_2, and K_3 are given in Eq. (7). The horizontal component of the descent engine thrust is a constant while the vertical thrust component is a linear function of time. A one-dimensional vertical descent of a lunar lander in a constant gravitational field to achieve zero velocity at TD with minimum fuel expenditure was formulated in Ref. 19. The resultant optimum control is also nearly a linear function of time.[19]

$$\begin{aligned}
&r = \frac{T}{W} \text{ (unitless)} \\
&\Delta = \frac{T^3}{3}(1+\frac{1}{4}r) \text{ (in units of } s^3) \\
&K_1 = \frac{x_{10}/W}{\{1+r\}} \quad \text{(in units of } m/s^2) \\
&K_2 = \frac{1}{\Delta}\{T(1+\frac{r}{2})x_{20} + (1+r)H_0 - \frac{g}{2}T^2\} \quad \text{(in units of } m/s^3) \\
&K_3 = \frac{T}{\Delta}\{T(1+\frac{r}{3})x_{20} + (1+\frac{r}{2})H_0 - \frac{g}{2}T^2(1+\frac{r}{6})\} \quad \text{(in units of } m/s^2) \\
&K_4 = K_3 + g \quad \text{(in units of } m/s^2)
\end{aligned} \tag{7}$$

The time histories of the horizontal velocity, vertical velocity, and that of the altitude are given by the following expressions:

$$\begin{aligned}
&x_1(t) = -K_1 t + x_{10} \\
&x_2(t) = \frac{1}{2}K_2 t^2 - K_4 t + x_{20} \\
&x_3(t) = \frac{1}{6}K_2 t^3 - \frac{1}{2}K_4 t^2 + x_{20} t + H_0
\end{aligned} \tag{8}$$

The resultant TD states of the lander (time = T) are given by the following expressions:

$$x_1(T)=\frac{x_{10}}{(1+r)}$$

$$x_2(T)=-\frac{3}{2T(1+\frac{r}{4})}(H_0+T\frac{x_{20}}{3}+\frac{g}{6}T^2) \tag{9}$$

$$\theta(T)=\tan^{-1}\{\frac{u_1(T)}{u_2(T)}\}=\tan^{-1}\{\frac{-2T(1+\frac{r}{4})x_{10}}{(1+r)\{Tx_{20}+3H_0+\frac{g}{2}T^2\}}\}$$

$$\text{Horizontal distance travelled} = \frac{x_{10}T}{2}\{\frac{2+r}{1+r}\}$$

A careful study of the expressions given in Eq. (9) can help us to gain insights into the essential features of the optimal solution. Given r, we observe that the horizontal TD velocity is proportional to x_{10} (the initial horizontal velocity of the vehicle). The vertical TD velocity is proportional to $\{H_0/T + x_{20}/3+ gT/6\}$. Note that if x_{20} is negative (downward velocity), the magnitude of the vertical TD velocity will actually be smaller than the vertical TD velocity with a positive x_{20}. This sounds counterintuitive. The reason is because some of the flight time T is "wasted" in negating the "upward" motion of the vehicle. Using the remaining flight time to cushion the landing will actually lead to a larger vertical TD velocity. As another example, let us consider the impact the acceleration due to gravity "g" have on the vertical TD velocity. From Eq. (9), we note that the vertical TD velocity is proportional to $\{H_0/T + x_{20}/3 + gT/6\}$. Using this relation, one can estimate the magnitude of the vertical TD velocity for landing on Mars (with $g \approx 3.69$ m/s^2) relative to that of landing on the Moon ($g \approx 1.634$ m/s^2).

$$u_1(t) = -0.185 \quad \text{m/s}^2$$
$$u_2(t) = 1.78265 - 0.00264 \times t \quad \text{m/s}^2 \tag{10}$$

The peak magnitude of the normalized engine thrust occurred at the start of the landing maneuver. Its magnitude is 1.7922 m/s^2. Assuming a mass of 20 metric ton, the peak magnitude of the physical thrust needed is 35,844 N. The corresponding throttle level is 43.3% (the peak thrust of the descent engine is 82,857 N). The resultant optimal trajectory is depicted in Fig. 4. The fuel cost of this optimization problem is computed as:

$$\Delta V\ (\text{m/s}) = \int_0^T \sqrt{u_1^2+u_2^2(t)}dt \tag{11}$$

Using Eqs. (10–11), the computed fuel cost is about 135.5 m/s. Again, assuming a landing mass of about 20 metric tons and an engine specific impulse of 448 s,[24] the fuel consumed is 616.9 kg. The total fuel consumed from the start of the powered descent and landing maneuver to TD (including the Braking, Approach, and Landing sub-phases) is estimated to be 11,000 kg.[24] The fuel cost for the landing and terminal descent sub-phase represents only 5.6% of the total fuel cost. This is why the fuel cost represents only part of the cost function in our formulated optimization problem (see Eq. (3)). Also, it only represents about 3.1% of the vehicle mass (at TD). Hence, the "constant mass" assumption we used in the formulation of the lunar landing optimization problem is reasonable.

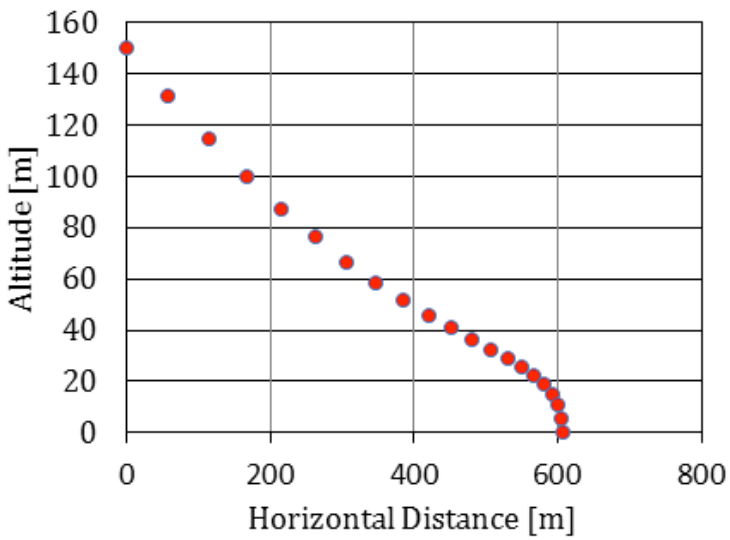

Fig. 4. Optimal landing trajectory.

The horizontal and vertical velocities of the lander at touchdown are 0.19 and –1.57 m/s (downward), respectively. This particular touchdown performance is well within the Apollo-11 TD envelope. The variations of these TD velocities with the weighting factor W are given in Fig. 5. The variations of the magnitudes of the touchdown velocities with the parameter r (=T/W) are given by Eq. (9). So, not surprisingly, the larger the weight W, the larger will be the TD velocities, and the smaller will be the fuel cost (cf. Fig. 6).

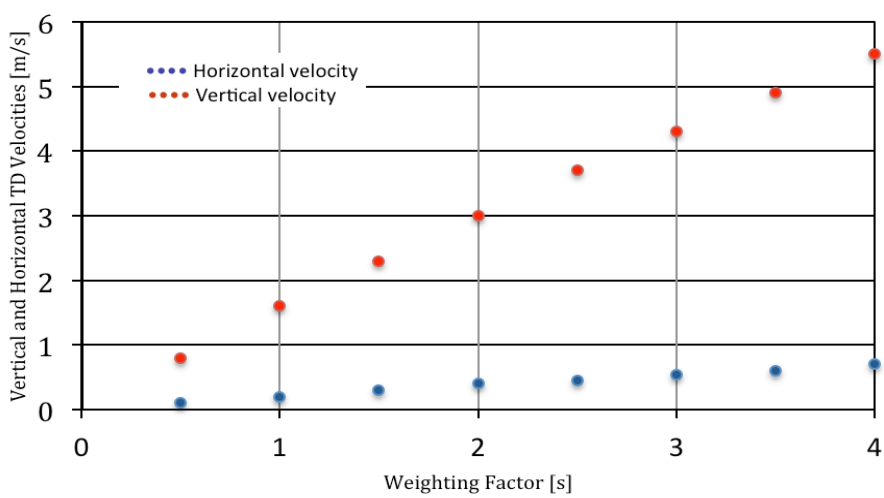

Fig. 5. The variations of the horizontal and vertical TD velocities with the weighting factor W.

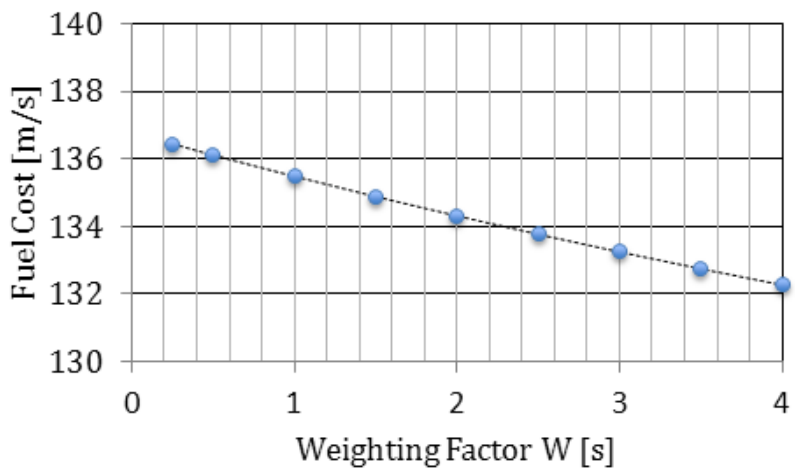

Fig. 6. The variations of the fuel cost with weighting factor W.

III. Optimal Control Problem with A "Hard" Terminal Downrange Constraint

At times, there is a need to constraint the lander to touch down at a fixed downrange "D" m from the initial position of the vehicle. That is, the initial and terminal states of x_4 are: $x_4(0) = 0$ and $x_4(T) = D$. The resultant optimal control for this revised problem is given by:

$$\begin{aligned} u_1(t) &= L_4 t - L_1 = \text{Linear variation of time} \\ u_2(t) &= L_2 t - L_3 = \text{Linear variation of time} \end{aligned} \tag{12}$$

$$\theta\,(t) = \tan^{-1}\{\frac{u_1}{u_2}\} = \tan^{-1}\{\frac{L_4 t - L_1}{L_2 t - L_3}\} = \text{Bilinear Tangent Law} \tag{13}$$

Here, the constants L_1, L_2, L_3, and L_4 are given in Eq. (14). The angle θ represents the deviation of the thrust vector from the local vertical. The structure of the optimal control has the familiar bilinear tangent law.[23] Without the hard downrange constraint, the bilinear tangent law becomes a linear tangent law (see Eq. (6)).

$$\begin{aligned} L_1 &= \frac{x_{10}/W}{(1+\frac{r}{4})} - \frac{T}{\Delta}\{D(1+\frac{r}{2}) - x_{10}T\} \text{ (in units of m/s}^2\text{)} \\ L_2 &= K_2 \text{ in equation (7) (in units of m/s}^3\text{)} \\ L_3 &= K_3 \text{ in equation (7) (in units of m/s}^2\text{)} \\ L_4 &= \frac{1}{\Delta}\{x_{10}T(1+\frac{r}{2}) - D(1+r)\} \text{ (in units of m/s}^3\text{)} \end{aligned} \tag{14}$$

The term Δ used in Eq. (14) was defined in Eq. (7). The resultant time histories of the horizontal and vertical velocities, and those of the altitude and downrange are given by the following expressions:

$$\begin{aligned} x_1(t) &= \frac{1}{2}L_4 t^2 - L_1 t + x_{10} \\ x_2(t) &= \frac{1}{2}L_2 t^2 - (L_3 + g)t + x_{20} \\ x_3(t) &= \frac{1}{6}L_2 t^3 - \frac{1}{2}(L_3 + g)t^2 + x_{20}t + H_0 \\ x_4(t) &= \frac{1}{6}L_4 t^3 - \frac{1}{2}L_1 t^2 + x_{10}t \end{aligned} \tag{15}$$

The resultant TD states of the lander are given by the following expressions:

$$
\begin{aligned}
x_1(T) &= \frac{1}{2(1+\frac{r}{4})}(3\frac{D}{T} - x_{10}) \\
x_2(T) &= -\frac{1}{2(1+\frac{r}{4})}(3\frac{H_0}{T} + x_{20} + \frac{g}{2}T) \\
\theta(T) &= \tan^{-1}\{\frac{u_1(T)}{u_2(T)}\} = \tan^{-1}\{\frac{x_{10}T - 3D}{Tx_{20} + 3H_0 + \frac{g}{2}T^2}\}
\end{aligned}
\tag{16}
$$

Note that the second expression of Eq. (16), on the vertical TD velocity, is identical to the second expression of Eq. (9). Looking at Eq. (12), we note that $u_1(t)$ becomes a constant term (cf. Eq. (6)) if L_4 is zero. Using the fourth expression of Eq. (14), we see that L_4 is zero if the terminal horizontal distance travelled $D = x_{10}T(1+r/2)/(1+r)$. But this is exactly the same expression for the terminal downrange given in Eq. (9) for the unconstrained optimization problem. Back substitution of this expression for D into the first expression of Eq. (14), we have $L_1 = x_{10}/W/\{1+r\}$, which is identical to the expression for K_1 in Eq. (7). Finally, we note that if $D = x_{10}T/3$, the angle between the thrust vector and the local vertical is zero, which is the desirable thrust direction at TD. If this condition is only approximately satisfied, the pitch angle at TD will be non-zero but small. Sometimes optimal descent and landing problems were formulated with a constraint of having a vertical thrust direction at the time of TD.[20] This constraint was not imposed in our study because a "hard" (or "soft") constraint on the TD downrange will indirectly cause the pitch angle at TD to be close to zero (see also Table 2). See also Section V.

Consider the same landing scenario with the following initial conditions: x_{10} = 15 m/s, x_{20} = –5 m/s, and H_0 = 150 m. The acceleration due to the lunar gravity is g = 1.634 m/s^2. Let the time given to TD T = 80 s, and the weighting factor W = 1 s (hence, r = T/W = 80). Let D be 400 m (the "low-gate" downrange selected for the Apollo-11 mission was 370 m. See Section I). The resultant optimal controls are given by:

$$
\begin{aligned}
u_1(t) &= -0.375 + 0.00469 \times t \qquad \text{m/s}^2 \\
u_2(t) &= 1.78265 - 0.00264 \times t \qquad \text{m/s}^2
\end{aligned}
\tag{17}
$$

Not surprisingly, $u_2(t)$ of the constrained problem is identical to the $u_2(t)$ of the unconstrained optimal control problem (see Eq. (10)). But unlike the constant $u_1(t)$ of the unconstrained optimal control problem, $u_1(t)$ of the constrained optimal control problem varies linearly with time. For about the first half of the flight time, the magnitude of $u_1(t)$ is larger than its counterpart computed via Eq. (10). This helps to brake the forward motion of the vehicle in order to touch down at a distance of 400 m (instead of the 607.4-m as computed for the unconstrained optimal control problem). The fuel cost of this optimization problem, with a hard downrange constraint, is 135.73 m/s. Not surprisingly, its magnitude is larger than that computed for the unconstrained optimization problem (but only slightly). The optimal trajectory is depicted in Fig. 7. Superimposed in Fig. 7 is the nominal descent trajectory of the Apollo-11 mission: Height and range to TD at the low gate were 155 m and 370 m. The terminal vertical descent started at an altitude of 30 m. Note that the optimal descent trajectory resembles that of the Apollo-11 mission, especially if we use D = 370 m (instead of 400 m) in the computation.

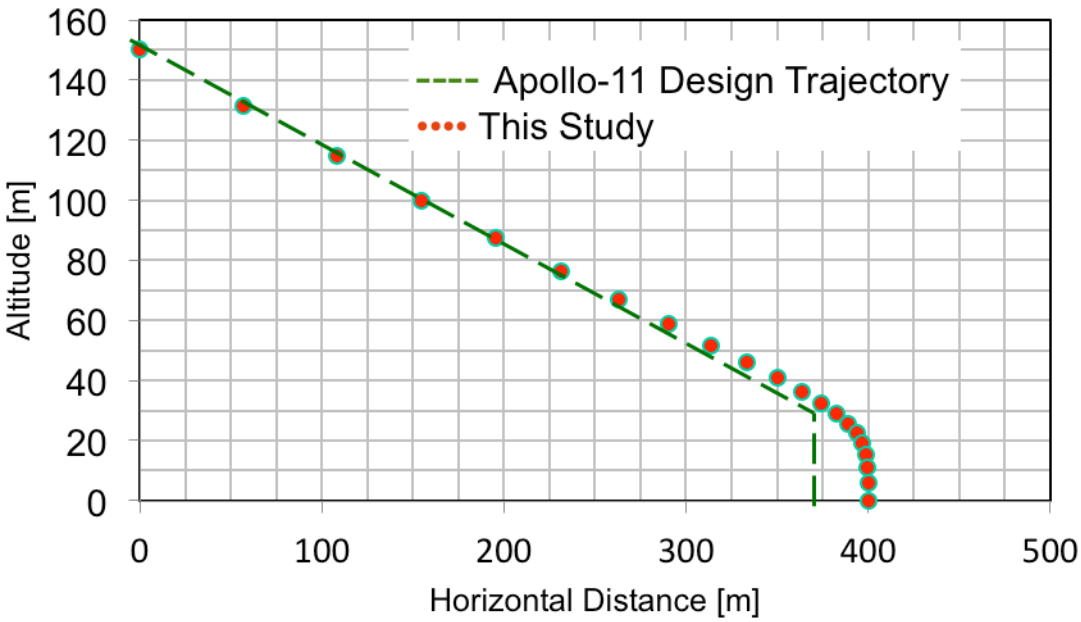

Fig. 7. Optimal descent trajectory.

IV. Optimal Control Problem with a "Soft" Terminal Downrange Constraint

There is an alternative way to constraint the lander to touch down at a downrange "D" m from the initial position of the vehicle. Instead of forcing the lander to touch down exactly with $x_4(T) = D$, we could guide it to achieve, "as close as possible", the condition $x_4(T) = D$. To this end, the cost function of Eq. (2) is modified as follows:

$$J = \frac{1}{2}[x_1^2(T) + x_2^2(T) + \alpha\{x_4(T)\text{-}D\}^2] + \frac{W}{2}\int_0^T [u_1^2(t) + u_2^2(t)]\, dt \tag{18}$$

Physically, the first component of J is related to the lander's TD velocity. The unit of this term is m^2/s^2. The weighting parameter α is positive and has units of s^{-2}. The addition of the α term is to guide the lander to land as close as possible with $x_4(T) = D$. The second component of J is related to the fuel cost as described in Eq. (2). The weighting parameter W, in units of seconds, is used to add the two terms together in the cost function. The resultant optimal control solution is:

$$\begin{aligned} u_1(t) &= L_4 t - L_1 = \text{Linear variation of time} \\ u_2(t) &= L_2 t - L_3 = \text{Linear variation of time} \\ \theta(t) &= \tan^{-1}\{\frac{u_1(t)}{u_2(t)}\} = \tan^{-1}\{\frac{L_4 t - L_1}{L_2 t - L_3}\} = \text{Bilinear Tangent Law} \end{aligned} \tag{19}$$

The structure of this bilinear tangent law is identical to that given in Eq. (13), but the constants L_1, L_2, L_3, and L_4 are given by the following new expressions:

$$
\begin{aligned}
L_1 &= \frac{\{2\alpha(1+\frac{r}{3})T^2+1\}x_{10} - 2T(1+\frac{r}{2})\alpha D\}}{2\alpha\Delta + T + W} \text{ (in units of m/s}^2\text{)} \\
L_2 &= K_2 \text{ in Eq. (7) (in units of m/s}^3\text{)} \\
L_3 &= K_3 \text{ in Eq. (7) (in units of m/s}^2\text{)} \\
L_4 &= \frac{\alpha\{(2+r)Tx_{10} - 2(1+r)D\}}{2\alpha\Delta + T + W} \text{ (in units of m/s}^3\text{)}
\end{aligned}
\tag{20}
$$

The term Δ used in Eq. (20) was defined in Eq. (7). Note that, if $\alpha = 0$, $L_4 = 0$ and $L_1 = K_1$ in Eq. (7). Accordingly, $u_1(t) = -L_1 = -K_1$, is a constant, as per that given by Eq. (6). The resultant TD states of the lander are given by the following expressions.

$$
\begin{aligned}
x_1(T) &= \{2\alpha\Delta+T+W\}^{-1}\{x_{10}(W-\frac{1}{3}\alpha T^3)+\alpha DT^2\} \\
x_2(T) &= -\frac{3}{2T(1+\frac{r}{4})}(H_0+T\frac{x_{20}}{3}+\frac{g}{6}T^2) \\
x_4(T) &= \{2\alpha\Delta+T+W\}^{-1}\{x_{10}WT(1+\frac{r}{2})+2\alpha\Delta D\} \\
\theta(T) &= \tan^{-1}\{\frac{2T^2(1+\frac{r}{4})[r\alpha T(\frac{1}{3}x_{10}T-D)-x_{10}]}{r\{Tx_{20}+3H_0+\frac{g}{2}T^2\}(2\alpha\Delta+T+W)}\}
\end{aligned}
\tag{21}
$$

Note that the vertical TD velocity is identical to that given in Eq. (9). The horizontal velocity at TD, for $\alpha = 0$, is also identical to that given in Eq. (9). Also, for $\alpha = 0$, the angle θ becomes identical to that given in Eq. (9).

Consider the same landing scenario considered in Section III. Let D be 400 m and $\alpha = 0.0005\ s^{-2}$. The optimal controls are given by Eq. (22), and the corresponding optimal trajectory is very similar to that given in Fig. 7.

$$
\begin{aligned}
u_1(t) &= -0.3708 + 0.00458 \times t \qquad m/s^2 \\
u_2(t) &= 1.78265 - 0.00264 \times t \qquad m/s^2
\end{aligned}
\tag{22}
$$

Note that, not surprisingly, the vertical thrust component $u_2(t)$ of this "soft" constrained problem is identical to the $u_2(t)$ of the unconstrained optimal control solution (see Eq. (10)) or that of the "hard" constraint optimal control solution (cf. Eq. (17)). But unlike the constant $u_1(t)$ of the unconstrained optimal control problem, the current optimal $u_1(t)$ at the start of the descent has a smaller value. As a result, the initial pitch angle in the "soft" constraint solution is smaller than that computed using the unconstrained optimal control solution (cf. Eq. (10). See Table 2. The fuel cost of this optimization problem, with a "soft" constraint on the terminal downrange is 135.72 m/s. Not surprisingly, its magnitude is larger than that computed for the unconstrained optimization problem, but smaller than that computed for the optimization problem with a "hard" downrange constraint. The terminal TD range is not exactly 400 m. It is 404.58 m. It is about 4.58 m away from the desired D = 400 m target. This deviation is as per that predicted in Eq. (21). The variation of the miss distance with respect to α is given in Fig. 8. A comparison of the landing and TD performance of the three guidance algorithms is given in Table 2.

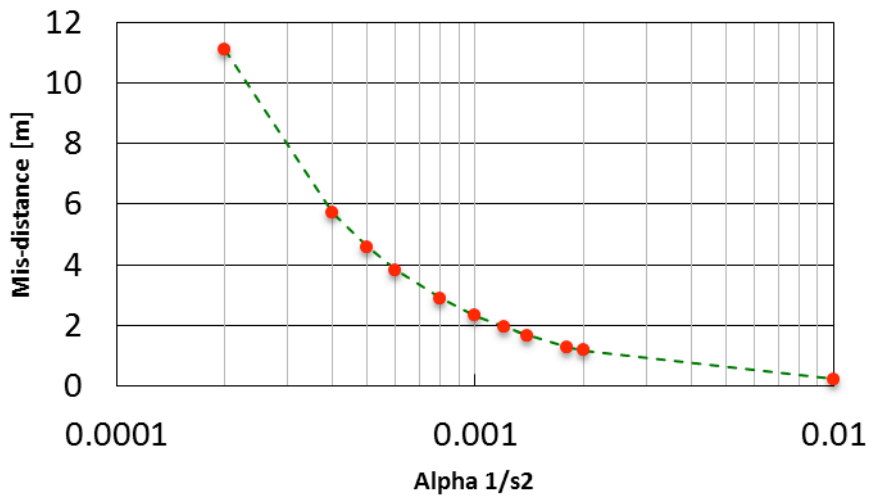

Fig. 8. Variation of miss-distance with α.

Table 2. Performance of Three Vehicle Landing and Touchdown Guidance Designs

Constraint on TD Downrange	Velocity [m/s]		Fuel Used [m/s]	Downrange at TD [m]	Pitch Angle [deg]	
	Vertical	Horizontal			Start	TD
None	1.57	0.19	135.50	607.4	5.93	6.96
Hard	1.57	0.00	135.73	400.0	11.4	0.0
Soft	1.60	0.004	135.72	404.6	11.3	0.1

V. Discussions

A cross plot of the lander's altitude versus its descent rate computed using the optimal control program (with a hard terminal distance constraint) is depicted in Fig. 9. It is compared with both the preflight landing trajectory design (solid green line) and the "abort boundary" of the Apollo-11 mission. In the first part of the Apollo-11 preflight trajectory design, the rate of descent was designed to decrease linearly with the altitude. The altitude and the rate of descent at the "low gate" were 155 m and 4.6 m/s, respectively. The altitude rate decreased gradually to a value of about 1.53 m/s at an altitude of 30 m. Thereafter, a 1.53-m/s descent rate was maintained in order to expedite the landing. At an altitude of about 15.3 m, the descent rate was further decreased in order to touch down with a lower velocity of 1.06 m/s.[‡]

The computed optimal control program also produces a descent rate that initially decreases linearly with altitude. At time ≈ 56.3 s, the descent rate reaches a minimum value of about 0.82 m/s at an altitude of 25.7 m. Thereafter, the optimal control program actually increases the descent rate in order to expedite the descent and the vehicle touchdowns with a descent rate of about 1.57 m/s (see also Eq. (16)). The "knee" of the computed optimal solution resembles the preflight landing trajectory design of Apollo-11. If a smaller weight factor W of 0.7 s is used, an even stronger resemblance between the computed optimal solution and its Apollo-11 counterpart was observed (cf. Fig. 10).

However, there is a critical difference between the computed optimal solution and its Apollo-11 counterpart. With the Apollo-11 design, the rate of descent decreases monotonically with altitude. That is, the lander has the lowest rate of descent at the time of TD. With the optimal control program, the lowest rate of descent achieved was 0.82 m/s when the lander was still 25.7 m from the ground. Thereafter, in order to expedite the landing, the optimal program actually drives the lander's rate of descent to increase, and the vehicle's TD velocity was 1.57 m/s (which is still acceptable per Eq. (1)). This optimal program is counter-intuitive and might not be acceptable to the crew.

In Figs. 9 and 10, the "Abort" boundary is applicable to situations in which the descent engine has to be cut off and the vehicle staged to abort on the ascent engine (with a 2-s time delay).[12] It is obvious that the abort boundary

[‡] The profile given in Fig. 9 is the preflight design. The actual profile, given in Fig. 11, deviated from the preflight design due to the re-designation of the landing site.

must be violated prior to effecting a landing. However, this boundary is violated only when the altitude is <25 m. This is considered acceptable.

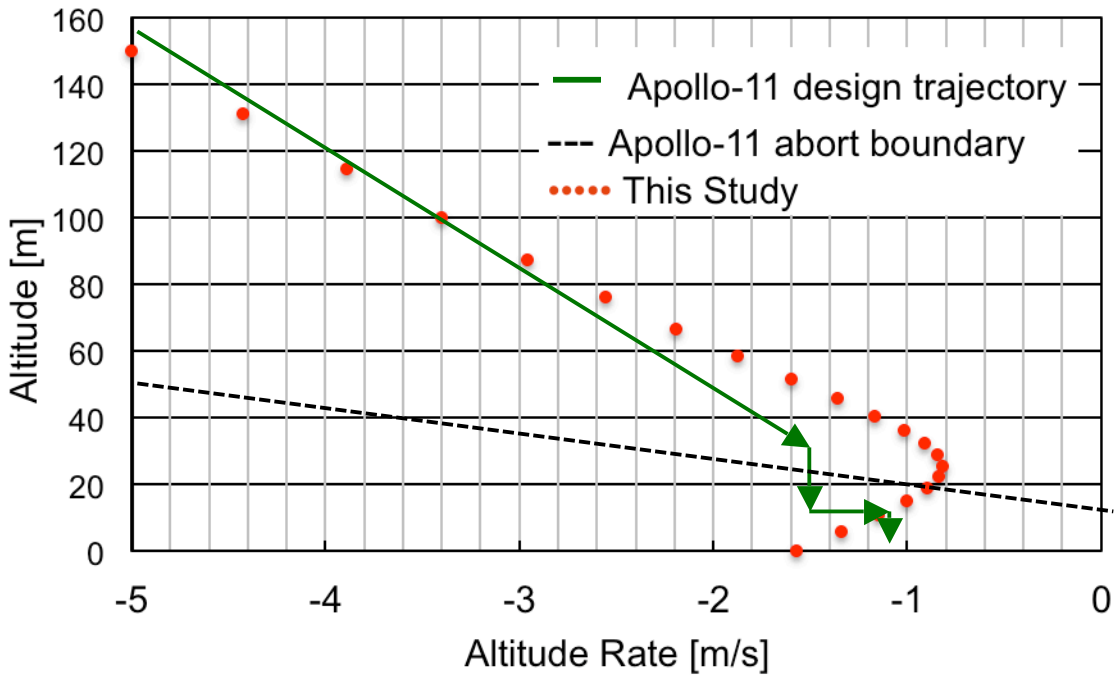

Fig. 9. Rate of descent vs. altitude for Apollo-11 design compared to study results (W = 1 s).

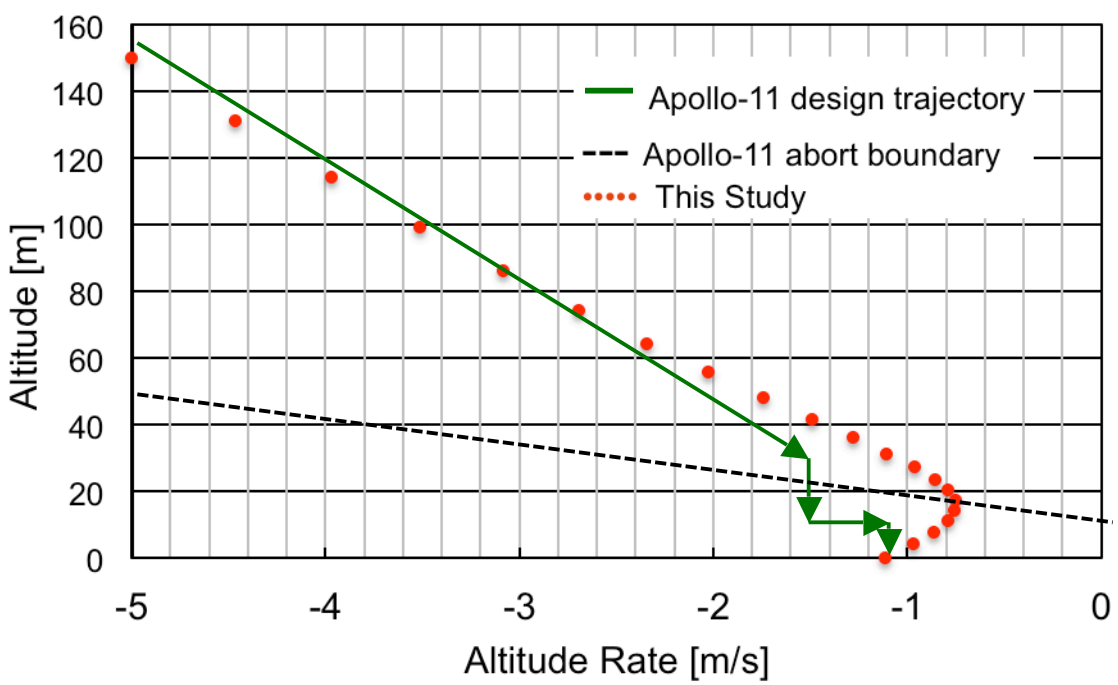

Fig. 10. Rate of descent vs. altitude for Apollo-11 design compared to study results (W = 0.7 s).

If we select D and H_0 to satisfy the relations: $3D=+x_{10}T$ and $3H_0= -x_{20}T$ (note that, typically, x_{20} has a negative value), then, using Eq. (16), we have:

$$\begin{aligned} &x_1(T)= 0 \\ &x_2(T)= -\frac{gT}{4(1+\frac{r}{4})} \approx -gW \text{ (if } r >>1) \\ &\theta(T)= 0 \end{aligned} \tag{23}$$

In Eq. (23), we note that both the lander's horizontal velocity and pitch angle are zero at TD, which is highly desirable. The lander's vertical velocity at TD is proportional to the weighting factor W. However, the TD scenario is complicated by the need to shut down the engine before the vehicle TD!

In April 1967, due to an error in the radar signal logic, the Surveyor III touchdown on the Moon with its vernier engine still firing.[25] The lander subsequently executed two rebounds on the lunar surface prior to receiving a thrust shutdown command from Mission Control. Because of this lesson learned, and a desire to limit erosion of the landing surface, a constraint of having the descent engine off at touchdown was widely accepted. For Apollo missions, engine shutdown was performed manually when 1.7-m contact probes touched the ground and a light was activated in the cockpit. The Altair landing gear does not currently include similar probes. The tentative plan is to shut down the engine at an altitude of 1 m. The altitude is to be estimated using measurements from the landing radar, the IMU, and the optical navigation system. If the estimation uncertainty of the altitude is unacceptably large, alternative solutions must be devised.

When the engine is shut down, its thrust will decay exponentially with a tail-off time constant of τ_{Tail} (assumed to be 0.150 s in this study). The time histories of the lander's vertical velocity and the distance it travelled after the engine has been shut down are given by:

$$\begin{aligned} &V(t) = V(0)+gt - \tau_{Tail}u_2^{shutdown}(1-e^{-\frac{t}{\tau_{Tail}}}) \\ &d(t) = \{V(0) - \tau_{Tail}u_2^{shutdown}\}t + \frac{1}{2}gt^2 - \tau_{Tailoff}^2 u_2^{shutdown}(1-e^{-\frac{t}{\tau_{Tail}}}) \end{aligned} \tag{24}$$

Here, V(t) is the lander's vertical velocity (measured positive downward) at time t (as measured from the time of engine shutdown), V(0) is the lander's vertical velocity at the time of engine shutdown, d(t) is the vertical distance travelled by the lander at time t (measured positive downward), and $u_2^{Shutdown}$ is the normalized vertical thrust at the time of engine shutdown. With W = 0.4 s (the selection of this particular weighting factor is made clear in following discussions), we have the following engine shutdown conditions from Eqs. (12–16): $u_2^{Shutdown}$ = 1.6173 m/s^2 and V(0) = 0.65 m/s. With these initial conditions, and using Eq. (24), the time for the lander to travel the last 1 m is 0.88 s, and the TD velocity is 1.843 m/s. The velocity increment, from the engine shutdown to TD, is 1.193 m/s. This velocity increment must be considered in the selection of the target vertical velocity at the time of engine shutdown.

From Eq. (1), we note that the maximum allowable vertical TD velocity for the Apollo landers was 3.05 m/s. Let us select the target TD condition for the Altair lander to be 60% of the maximum value: 3.05×0.6=1.83 m/s. Accordingly, the lander's vertical velocity at the time of engine shutdown must not exceed 1.83–1.193 = 0.637 m/s. To achieve this vertical velocity, according to Eq. (23), we need a weighting factor of W = 0.637/1.634 ≈ 0.4.

Using the same conditions $3D = +x_{10}T$ and $3H_0 = -x_{20}T$, the optimal control programs are given by (cf. Eqs. (7) and (14)).

$$\begin{aligned} &u_1(t)=\frac{2x_{10}}{T}(\frac{t}{T}-1) \\ &u_2(t)=\{\frac{2x_{20}}{T}-\frac{3g}{2(1+\frac{r}{4})}\}(\frac{t}{T}-1)+\frac{gr}{4(1+\frac{r}{4})} \approx \frac{2}{T}\{x_{20}-3gW\}(\frac{t}{T}-1)+g \qquad \text{(if } r >>1) \end{aligned} \tag{25}$$

The pitch angle of the lander at the start of the Descent and Landing sub-phase must match the pitch angle at the end of the Approach sub-phase (denotes by $\phi_{Approach}$). Matching the pitch angle at the interface of the two sub-phases will provide us with an estimate of the maneuver time T.

$$\theta(0)=\tan^{-1}\{\frac{u_1(0)}{u_2(0)}\}=\tan^{-1}\{\frac{-\frac{2x_{10}}{T}}{-\frac{2x_{20}}{T}+\frac{g(r+6)}{(r+4)}}\}=\tan^{-1}\{\frac{-2x_{10}}{-2x_{20}+gT}\}=-\phi_{\text{Approach}} \qquad (\text{if } r>>1) \tag{26}$$

$$T=\frac{2}{g\tan\phi_{\text{Approach}}^{T}}\{x_{10}+\tan\phi_{\text{Approach}}x_{20}\}$$

For the Apollo-11 mission, ϕ_{Approach} was 11° (backward). Using the second expression in Eq. (26), and with x_{10} = 15 m/s and x_{20} = –5 m/s, the computed maneuver time T is 88.5 s. With this maneuver time, the computed downrange D = $1/3x_{10}T=1/3(15\times88.5)$= 442.5 m, the altitude of the "low gate" is $H_0 = -1/3x_{20}T$=147.5 m. A comparison of the preflight design values of the "low gate" conditions of the Apollo-11 mission and those computed via Eqs. (23–26) is given in Table 3. Note that the magnitudes of the ratios $D/(x_{10}T)$ and $H_0/(|x_{20}|T)$ for the Apollo-11 preflight design are:

$$\frac{D}{x_{10}T}=\frac{370}{16\times80}=0.289\approx\frac{1}{3} \tag{27}$$
$$\frac{H_0}{|x_{20}|T}=\frac{155}{4.8\times80}=0.404\approx\frac{1}{3}$$

Table 3. Landing Conditions of Apollo-11 Preflight Landing Trajectory Design and Those Computed in This Study

Mission	Initial Horizontal Velocity [m/s]	Initial Vertical Velocity [m/s]	Time to TD [s]	Down Range [m]	Initial Altitude [m]	Initial Pitch Angle [deg]	TD Pitch Angle [deg]	TD Horizontal Velocity [m/s]	TD Vertical Velocity [m/s]	Fuel Used [m/s]
This Study	15	5	88.5	442.5	147.5	11	0	0	1.846[a]	136.6
Apollo-11 [preflight]	16	4.8	80	370	155	11	0	0	1.05[b]	119+100[c]

[a]The near touchdown vertical velocity is 0.65 m/s. The ΔV due to 1-m free fall is 1.193 m/s. The resultant TD velocity is 1.846 m/s.
[b]This TD velocity does not include the component due to the free fall of the vehicle.
[c]This nominal ΔV budget for the Apollo landing phase is 119 m/s. The contingency ΔV budget is 100 m/s.

From Eq. (23), we note that if D and H_0 satisfy the following relations: $3D = +x_{10}T$ and $3H_0 = |x_{20}|T$, then, both the horizontal velocity and pitch angle at TD are zero, and the vertical TD velocity is small. The low-gate condition selected for the preflight landing trajectory design for the Apollo-11 mission approximates these conditions. The actual landing time T of the Apollo-11 mission was 140 s. It is significantly longer than the preflight design value of 80 s. This is because the crew detected roughness in the vicinity of the targeted landing site and took evasive actions. The crew was also distracted by three detected computer-fault alarms and one detected "propellant low" condition. The cross plot of the actual altitude vs. altitude rate of the Apollo-11 mission is given in Fig. 11. Obviously, the ratios $D/(x_{10}T)$ and $H_0/(|x_{20}|T)$ do not approximate ⅓.

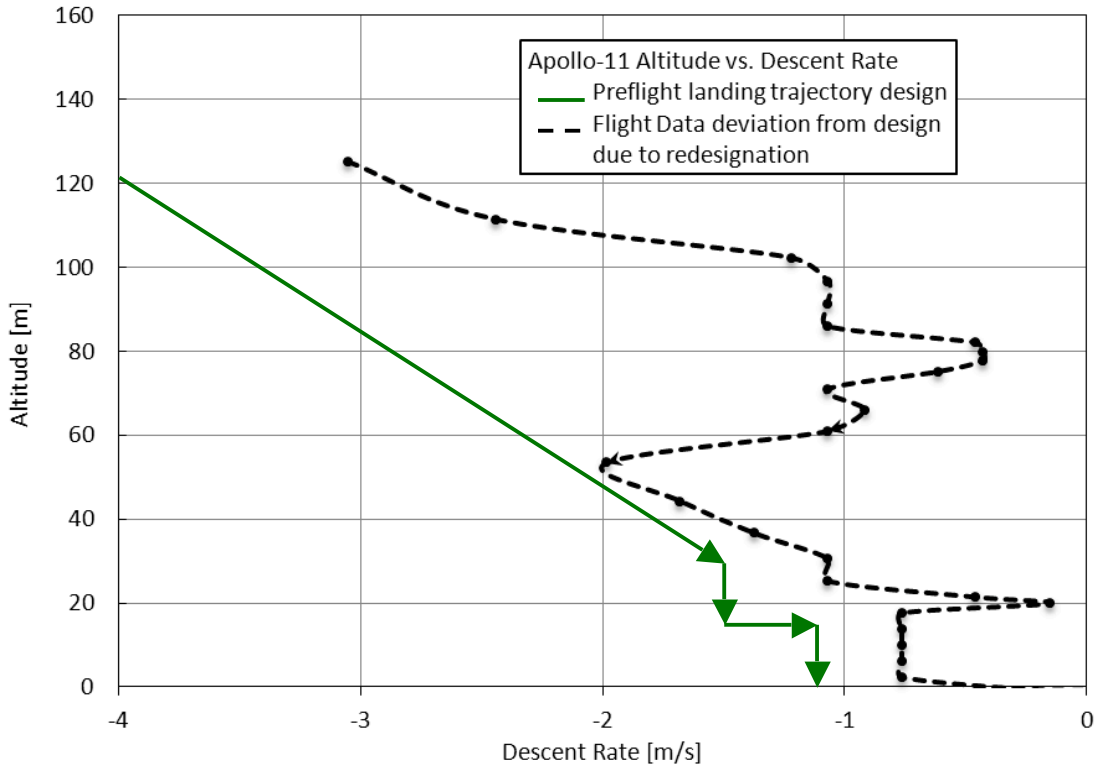

Fig. 11. Apollo-11 flight data: altitude vs. altitude rate (Reconstructed Using Flight Data from Ref. 8).

VI. Conclusions

In this study, the optimal control of a lander is formulated with a cost function that penalizes both the TD velocity and the fuel cost of the descent engine. With only a "soft" bound on the engine thrust (via the fuel cost), the optimal thrust components are continuous, linear functions of time. With this formulation, we can easily derive analytical expressions that relate the TD velocity components with the entry condition of the lander together with the flight time. Using these expressions, we note that if the downrange D and altitude H_0 at the entry of the Landing and Terminal Descent sub-phase satisfy the following relations: $3D = V_{Hori}^{Entry} T$ and $3H_0 = V_{Vertical}^{Entry} T$, then, both the horizontal and vertical velocities of the lander and its pitch angle at TD will be very small. It is interesting to note that the preflight landing trajectory design of the Apollo-11 mission satisfies these relations approximately. The actual landing trajectory of Apollo-11 mission deviated from these relations due to landing target redesignations executed by the lunar module pilot.

Acknowledgments

The work described in this paper was carried out by Jet Propulsion Laboratory, California Institute of Technology, under a contract with the National Aeronautics and Space Administration. Reference to any specific commercial product, process, or service by trade name, trademark, manufacturer, or otherwise, does not constitute or imply its endorsement by the United States Government or the Jet Propulsion Laboratory, California Institute of Technology. The publication of this paper does not constitute approval by NASA or JPL of the findings or the conclusions contained herein. It is published for the exchange and stimulation of ideas only. I am grateful to John M. Carson, III (at Jet Propulsion Laboratory), Ellen Braden, Brian Derkowski, Jonathan Lenius, and Alan Strahan (at NASA Johnson Space Center); Kendall Brown and Larry Kos (at NASA Marshall Space Flight Center); as well as

Tim Collins (at NASA Langley Research Center) for many helpful assists. I would also like to thank the two anonymous AIAA reviewers for their comments on an earlier draft of this paper.

References

[1]Lee, A.Y., Ely, T., Sostaric, R., Strahan, A., Riedel, J.E., Ingham, M., Wincentsen, J., and Sarani, S., "Preliminary Design of the Guidance, Navigation, and Control System of The Altair Lunar Lander," *AIAA-2010-7717, Proceedings of the AIAA Guidance, Navigation, and Control Conference,* Toronto, Ontario, Canada, August 2–5, 2010.

[2]Riedel, J. E., Ely, T., Lee, A. Y., Werner, R. A., Wang, T. C., Vaughan, A. T., Nolet, S., Myers, D. M., Mastrodemos, N., and Grasso, C., "Optical Navigation Plan and Strategy for the Lunar Lander Altair," *Proceedings of the AIAA Guidance, Navigation, and Control Conference, and Exhibit*, Toronto, Ontario, Canada, August 2–5, 2010.

[3]Strahan, A. L. and Johnson, A., "Terrain Hazard Detection and Avoidance during the Descent and Landing Phase of the Lunar Lander Altair Mission," *Proceedings of the AIAA Guidance, Navigation, and Control Conference, and Exhibit*, Toronto, Ontario, Canada, August 2–5, 2010.

[4]Epp, C. D., Robertson, E. A., and Brady, T., "Autonomous Landing and Hazard Avoidance Technology (ALHAT)," Paper 1501, *IEEE 2008 Aerospace Conference*, Big Sky, Montana, March 1–8, 2008.

[5]Sostaric, R., "Powered Descent Trajectory Guidance and Some Considerations for Human Lunar Landing," *Proceedings of the 30th Annual AAS Guidance and Control Conference*, Breckenridge, Colorado, February 3–7, 2007, AAS 07-051.

[6]Sullivan, J.J., Lee, A.Y., and Grover, M.R., "Rendezvous and Docking Sensor and Effector System Design Considerations for the Lunar Lander Altair," AIAA-2010-7723, *Proceedings of the AIAA Guidance, Navigation, and Control Conference,* Toronto, Ontario, Canada, August 2–5, 2010.

[7]Bennett, F.V., "Lunar Descent and Ascent Trajectories," AIAA Paper 70-25, *AIAA 8th Aerospace Sciences Meeting*, New York, New York January 19–21, 1970.

[8]NASA Manned Spacecraft Center, *Apollo 11 Guidance, Navigation and Control System Performance Analysis Report,* 11176-H433-R0-00, Project Technical Report, Task E-38C, NAS 9-8166, December 31, 1969.

[9]NASA Manned Spacecraft Center, *Apollo 12 Guidance, Navigation and Control System Performance Analysis Report*, 11176-H524-R0-00, Project Technical Report, Task E-38C, NAS 9-8166, April 8, 1970.

[10]NASA Manned Spacecraft Center, *Apollo 14 Guidance, Navigation and Control System Performance Analysis Report,* MSC-04112 Supplement 1, Project Technical Report, Task E-38C, NAS 9-8166, January 1972.

[11]Kos, L.D., Polsgrove, T.P., Sostaric, R.R., Braden, E.M., Sullivan, J. J., and Le, T. T., "Altair Descent and Ascent Reference Trajectory Design and Initial Dispersion Analyses," *Proceedings of the AIAA Guidance, Navigation, and Control Conference, and Exhibit*, Toronto, Ontario, Canada, August 2–5, 2010.

[12]Cheatham, D.C and Bennet, F.V., "Apollo Lunar Module Landing Strategy," *Apollo Lunar Landing Mission Symposium*, NASA TM-X-58006, June 1966, pp. 175–240.

[13]Rogers, W.F., *Apollo Experience Report – Lunar Module Landing Gear Subsystem*, NASA TN D-6850, Manned Spacecraft Center, Houston, Texas, June 1972.

[14]Hilderman, R.H., Mueller, W.H., and Mantus, M., "Landing Dynamics of the Lunar Excursion Module," *Journal of Spacecraft and Rockets*, Vol. 3, No. 10, October 1966, pp. 1484–1489.

[15]Lee, A.Y., Bryson, A.E., and Hindson, W.S., "Optimal Landing of a Helicopter in Autorotation," AIAA *Journal of Guidance, Control, and Dynamics*, Vol. 11, No. 1, January–February 1988, pp. 7–12.

[16]Lee, A.Y., "Optimal Autorotational Descent of a Helicopter with Control and State Inequality Constraints," AIAA *Journal of Guidance, Control, and Dynamics*, Vol. 13, No. 5, September-October 1990, pp. 922–924.

[17]Ploen, S.R., Acikmese, A.B., and Wolf, A., "A Comparison of Powered Descent Guidance Laws for Mars Pinpoint Landing," AIAA-2006-6676, *Proceedings of the AIAA/AAS Astrodynamics Specialist Conference*, Keystone, Colorado, August 21–24, 2006.

[18]Meditch, J.S., "On the Problem of Optimal Thrust Programming For a Lunar Soft Landing," *IEEE Transactions of Automatic Control*, Vol. AC-9, No. 4, 1964, pp. 477–484.

[19]Teng, L. and Kumar, K.S.P., "Optimum Control for Lunar Soft Landing," *Astronautica ACTA*, Vol. 13, 1968, pp. 531–545.

[20]Topcu, U., Casoliva, J., and Mease, K., "Minimum-Fuel Powered Descent for Mars Pinpoint Landing," *Journal of Spacecraft and Rockets*, Vol. 44, No. 2, March-April, 2007, pp. 324–331.

[21]D'Souza, C.N., "An Optimal Guidance Law for Planetary Landing," *Proceedings of the AIAA Guidance, Navigation, and Control Conference, and Exhibit*, New Orleans, LA, August 1997, AIAA 1997-3709.

[22]Rea, J.R. and Bishop, R.H., "Analytical Dimensional Reduction of a Fuel Optimal Powered Descent Sub-problem," *AIAA-2010-8026, Proceedings of the AIAA Guidance, Navigation, and Control Conference,* Toronto, Ontario, Canada, August 2–5, 2010.

[23]Bryson, A.E. and Ho, Y.C., "Applied Optimal Control," Hemisphere Publishing Corporation, Bristol, Pennsylvania, 1975.

[24]Lee, A. Y., Strahan, A., Tanimoto, R., and Casillas, A., "Preliminary Characterization of the Altair Lunar Lander Slosh Dynamics and Some Implications for the Thrust Vector Control Design," AIAA-2010-7721, *Proceedings of the AIAA Guidance, Navigation, and Control Conference,* Toronto, Ontario, Canada, August 2–5, 2010.

[25]Thurman, S., "Surveyor Spacecraft Automatic Landing System," *Advances in the Astronautical Sciences, Guidance and Control 2004*, Vol. 118, *Proceedings of the 27th Annual AAS Rocky Mountain Guidance and Control Conference*, February 4–8, 2004, Breckenridge, Colorado, pp. 427–437.